HHS Public Access

Author manuscript

Stem Cells. Author manuscript; available in PMC 2018 September 01.

Published in final edited form as:

Stem Cells. 2018 March ; 36(3): 349–362. doi:10.1002/stem.2746.

Low osteogenic yield in human pluripotent stem cells associates with differential neural crest promoter methylation

Nicole Renee Lee Sparks, **Ivann Kenneth Carvajal Martinez**, **Cristina Helen Soto**, and **Nicole Isolde zur Nieden**

Department of Molecular, Cell & Systems Biology and Stem Cell Center, College of Natural and Agricultural Sciences, University of California Riverside, Riverside, CA, 92521

SUMMARY

Human pluripotent stem cell-derived osteoblasts possess great potential for utilization in bone disorder elucidation and repair; yet, while the general ability of human pluripotent stem cells to differentiate into osteoblasts and lay down bone-specific matrix has been shown, previous studies lack the complete characterization of the process whereby such osteoblasts are derived as well as a comparison between the osteogenic efficiency of multiple cell lines. Here, we compared the osteogenic potential of two human induced pluripotent stem cell lines (RIV9 and RIV4) to human H9 embryonic stem cells. Generally capable of osteogenic differentiation, the overall osteogenic yield was lower in the RIV9 and RIV4 lines and correlated with differential expression of osteocalcin (*OCN*) in mature cultures and *PAX7* and *TWIST1* during early differentiation. In the undifferentiated cells the promoters of the latter two genes were differentially methylated potentially explaining the variation in differentiation efficiency. Furthermore, the expression signatures of selected neural crest and mesodermal genes and proteins suggested that H9 cells preferentially gave rise to neural crest-derived osteoblasts, whereas the osteoblasts in the RIV9 cultures were generated both through a mesodermal and a neural crest route albeit each at a lower rate. These data suggest that epigenetic dissimilarities between multiple PSC lines may lead to differences in lineage derivation and mineralization. Since osteoblast progenitors from one origin inadequately repair a defect in the other, these data underscore the importance of screening human pluripotent stem cells lines for the identity of the osteoprogenitors they lay down.

Summary of the study

The methylation status of the neural crest-associated *TWIST1* and *PAX7* promoters in undifferentiated human pluripotent stem cells predicts whether they will differentiate into neural-crest or mesoderm-derived osteoblasts. T/BRA, T-Brachyury.

CORRESPONDING AUTHOR: Nicole I. zur Nieden, 1113 Biological Sciences Building, Department of Molecular, Cell & Systems Biology and Stem Cell Center, College of Natural and Agricultural Sciences, University of California Riverside, Riverside, CA, 92521. nicolezn@ucr.edu, Tel: 951-827-3818.

AUTHOR CONTRIBUTIONS

NzN conceived and designed the study, analyzed and interpreted data, and drafted the manuscript. NRLS analyzed and interpreted data, drafted the manuscript and acquired most of the data. IKCM assisted with H9 analysis. CHS performed partial analysis of RIV4 hiPSCs. All authors critically revised the manuscript.

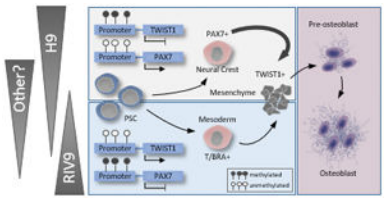

Keywords

human pluripotent stem cell; human induced pluripotent stem cell; osteoblast; calcification; neural crest

INTRODUCTION

The *in vitro* differentiation of human embryonic stem cells (hESCs) offers an invaluable source to study cellular development, the etiology of degenerative diseases, and the regeneration of dysfunctional tissues [1–4]. Human ESCs are exceptionally appropriate for the *in vitro* generation of specialized cells due to their pluripotency. Researchers have developed *in vitro* protocols that differentiate ESCs from mouse [5–7] and human [7–9] into functional osteoblasts that can mineralize their extracellular matrix (ECM), a hallmark of bone formation. Directed differentiation of ESCs towards an osteoblast lineage has been achieved using dexamethasone (DEX), which triggers the expression of the osteogenic genes runt-related transcription factor 2 (*RUNX2*) and osteocalcin (*OCN)* [10, 11]. Our group routinely uses the active exogenous factor 1α,25 dihydroxy vitamin D_3 (VD_3) to enhance commitment of mouse or primate ESCs towards the osteoblast lineage [6, 7, 12].

However, the ethical concerns surrounding the use of hESCs have held back exploring the great expectations otherwise associated with hESCs. Human induced pluripotent stem cells (hiPSCs), generated from the reprogramming of somatic cells, are also truly pluripotent cells and provide an alternative mean to obtain ES-like cells [13,14]. While believed to be broadly equivalent to hESCs based on morphology and gene expression [15–17], several reports have identified hiPSC lines to be different from hESCs in DNA methylation and gene expression signatures [18–21].

Increasingly, the capacity of iPSCs to differentiate into osteoblasts is at the center of studies, as these cells may be used in cell-based replacement therapies or embryotoxicity screening assays [22, 23]. To direct osteogenic differentiation in hiPSCs prior studies employed DEX addition to the culture medium or seeding these cells on three-dimensional (3D) scaffolds [24–32]. While these studies have provided evidence that hiPSCs are generally capable of generating osteoblasts they have not characterized whether they do so with a similar efficiency as hESCs and whether they do so through the same process. This is important, because osteoblasts may originate from the neural crest or the mesoderm, the former having superior grafting abilities than the latter [33, 34]. Similarly, a culture process which derives osteoblasts from the neural crest may not be suitable to uncover embryotoxicants that cause limb malformations *in vivo*.

As it is thus clearly necessary to elucidate the efficacy of hiPSC technology prior to routine experimental utilization of these cells [35], here we compared the osteogenic differentiation potential of two hiPSC lines, RIV9 and RIV4, with hESCs of the H9 line. Although RIV9 and RIV4 cells were generally capable of differentiating into functional matrix-calcifying osteoblasts when induced with VD_3, both of the hiPSC lines tested exhibited a lower potential to yield osteoblasts than the H9 cells as determined by bone-specific mRNA expression and quantification of calcium accumulation. Despite their lower differentiation potential, osteogenically induced RIV9 cells were equally sensitive to the strong embryotoxicant 5-Fluorouracil indicating their potential usefulness for the screening and identification of putative skeletal toxicants.

However, in H9 hESCs, VD_3 induction seemed to cause osteoblasts to form from a source of neural crest cells, while RIV9 osteoblasts seemed to be specified primarily from mesoderm and to a lesser degree the neural crest, whereas RIV4 cells seemed to prefer a neuroepithelial path. Differentiation efficiency and route was not inherently associated with the type of pluripotent stem cell, but rather seemingly correlated with the methylation state of neural crest promoters that was found before differentiation was initiated. In summary, our results indicate that before individual hPSC lines can come to use in orthopedic regenerative medicine or for the study of molecular mechanisms accompanying osteogenic differentiation, they need to be thoroughly characterized for the lineage origin they derive osteoblasts from.

MATERIALS AND METHODS

Human pluripotent stem cell lines

Cells of the hESC H9 line were acquired from WiCell (WiCell Research Institute). RIV4 and RIV9 hiPSCs were generated from foreskin fibroblasts (HFF-1, ATCC) by retroviral integration of *OCT4*, *KLF4* and *SOX2* at the University of California Riverside's Stem Cell Core Facility [36, 37]. To disrupt expression of T/Brachyury, human pluripotent stem cells (4×10^5 cells) were transfected with 0.3 μg brachyury CRISPR/Cas9 KO plasmid (h; sc-416539) and 0.3 μg brachyury HDR plasmid (h; sc-416539-HDR) from Santa Cruz using Effectene Transfection Reagent (Qiagen 301427). After 72 hours, transfectants were selected with 150 μg/ml puromycin (Sigma-Aldrich P8833) of for 3–5 days. Resistant colonies that were double positive for green and red fluorescent protein were picked and expanded for analysis. Osteogenic differentiation was conducted from those clones, in which a reduction in BRACHYURY protein expression during differentiation was confirmed. Control clones were generated using 0.3 μg Control CRISPR/Cas 9 plasmid. All cells were maintained on Matrigel (BD Biosciences) treated dishes in mTeSR® (Stem Cell Technologies) in 5% CO_2 and at 37°C. Pluripotent colonies were passaged every 5 days upon reaching 70% confluency by dissociating cells with accutase and a cell scraper.

Karyotyping

Standard G-banding type chromosome and cytogenetic analysis were carried out at the WiCell Research Institute.

Osteogenic Differentiation of hPSCs

Confluent pluripotent colonies (designated day 0) were switched to control differentiation medium composed of Dulbecco's Modified Medium (DMEM, Gibco) containing 15% FBS (Atlanta), 1% non-essential amino acids (NEAA; Gibco), 1:200 penicillin/streptomycin (Gibco), and 0.1 mM β-mercaptoethanol (Sigma). On day 5, control differentiation medium was supplemented with 10 mM β-glycerophosphate (Sigma), 50 μg/ml ascorbic acid (Sigma), and 50 nM 1,25$(OH)_2$ Vitamin D_3 (Calbiochem) [38].

Immunocytochemistry

Cells were fixed with 4% paraformaldehyde for 30 min at 4°C. After washing and permeabilizing (intracellular markers only) with 0.1% Triton-X 100 (Sigma) for 15 min, cells were incubated in primary antibody diluted in PBS/10% FBS overnight at 4°C. Primary antibodies used were POU5F1 (EMD Millipore, ab3209), NANOG (Cell Signaling 4903), SOX2 (Cell Signaling, 3579), SSEA4 (EMD Millipore, MAB4304), OCN (AbCam, ab1857), $p75^{NTR}$ (AbCam, ab8874), SOX10 (Santa Cruz, SC17342), TWIST1 (AbCam, ab50887), PDGRFα (AbCam, ab61216), and PAX7 [39] (mIgG1, Developmental Studies Hybridoma Bank). Cells were then washed and incubated in the appropriate secondary antibody (AlexaFluor conjugated) for 2h. Cells were observed on a Nikon fluorescent microscope.

Histochemical analysis

Cultures were washed with PBS and fixed in 4% paraformaldehyde at 4°C for 30 min. For Von Kossa stain, fixed samples were overlaid with silver nitrate solution (Ricca Chemical Company) and illuminated under an intense light source for 1 h. Cultures were fixed with 5% sodium thiosulfate (Red Bird Service) for 2 minutes. Cells were also washed with PBS and overlaid with 2% w/v Alizarin Red S solution (Sigma-Aldrich) for 5 minutes to visualize calcium-rich areas. Prior to imaging, cultures were washed 3X with water followed by ascending alcohol washes (70%, 80%, 90%, 100% ethanol).

Characterization of bone: Alkaline phosphatase (ALP), inorganic phosphate, and calcium assays

Cells were harvested in radioimmunoprecipitation (RIPA) buffer. Activity of the ALP enzyme and calcium deposition were determined and calculated as previously described [40]. Free inorganic phosphate (P_i) was measured with the PiPer phosphate assay (Molecular Probes, Invitrogen) per the protocol of the manufacturer and as used by Majumdar et al. [41]. The total free inorganic phosphate in the sample was taken from a potassium phosphate standard curve. All measurements were normalized to the total protein content of the sample measured with the Lowry method.

RNA isolation and quantitative PCR

Total RNA was extracted with the NucleoSpin RNA II protocol (Macherey Nagel). RNA concentration was determined with a NanoDrop® 1000 spectrophotometer (Thermo Scientific) at 260 nm. 25 ng of total RNA was used for cDNA synthesis with a mastermix including 1X reaction buffer, 0.5 mM dNTPs, 20 U/μL RNase inhibitor, 0.8 U/μL reverse

transcriptase, and 1 μM random primer. 25ng cDNA transcripts were used for quantitative polymerase chain reaction (qPCR) with SYBR green on the MyiQ cycler (BIO-RAD). Reactions were setup for 10 minutes of denaturing at 94°C, followed by 40 cycles of denaturing at 94°C, and annealing/elongation at 60°C for 45 seconds. The n-fold expression in target samples was calculated with the $\Delta\Delta C_T$ method by standardizing C_T values to *GAPDH* expression [42]. Primer sequences used in this study can be found in Supplemental Table 1. Pre-designed primer pairs for *GOOSECOID* (*GSC*; Hs00906630_g1), *PAX6* (Hs00240871_m1), and *SOX17* (Hs00751752_s1) were purchased from Life Technologies. All other primers were from Leung et al., 2016 [43].

Methylation-specific (MS) PCR Analysis

To analyze the methylation status of the *TWIST1* and *PAX7* promoters, cells were collected in lysis buffer (100 mM NaCl, 0.5% SDS, 20 mM Tris pH7.5, 50 mM EDTA) with 0.2 mg of proteinase K (Sigma) and incubated at 60°C overnight. DNA was isolated by standard phenol-chloroform and isopropanol precipitation methods and quantified with a NanoDrop® 1000 spectrophotometer. Bisulfite conversion was performed from 200 ng of genomic DNA with the EZ DNA Methylation-Lightning Kit (Zymo). The methylation status of the *PAX7* and *TWIST1* promoters was then determined from the eluted DNA using the MS-nested PCR method [44]. Primer sequences for first and second rounds of amplification for both methylated and unmethylated DNA are listed in Supplemental Table 1 and are as previously published [44]. Cycling conditions for *PAX7* were 10 minutes at 95°C, followed by 40 cycles at 94°C for 25 seconds, 60°C for 25 seconds, and 72°C for 20 seconds. A final elongation of 2 minutes at 72°C followed. The first and second reactions for *TWIST1* were setup for 10 minutes at 95°C, followed by 40 cycles for round one and 32 cycles in round 2 at 94°C for 25 seconds, 63.9°C for 25 seconds, 72°C for 20 seconds, and a final 2 minute elongation at 72°C. Amplified products were observed in a 2% agarose gel using ethidium bromide for detection.

MTT assay

Cellular health was determined with 3-[4,5-dimethylthiazol-2-yl]-2,5-diphenylterazolium bromide (MTT) as described previously [45] and absorbance was read at 595 nm in an iMark™ microplate reader (BIO-RAD).

Video bioinformatics

Phase contrast microscopic images of differentiating hPSCs were automatically acquired at a magnification of 4X every 12h utilizing the BioStation CT (Nikon Corporation, Tokyo, Japan). For each 24-well dish well ten reference points of interest were randomly selected as representative view fields. Raw images were processed, enhanced and segmented using MATLAB software-generated recipes (Mathworks, MA, U.S.A) using a manual threshold of 33. Pixels below the threshold were removed to create segmented images of calcified regions. Remaining pixels were counted to quantitatively represent the degree of calcification from each image. The calcification rate was determined from the number of calcified pixels in each image at t_x subtracted from the number of calcified pixels at t_0 and divided by the hours of elapsed time.

Toxicity Testing

5-Fluorouracil (5FU) was obtained from Sigma-Aldrich and a stock solution prepared in dimethyl sulfoxide. Differentiation of hPSCs was initiated as described above and cells were treated for 20 days of osteogenesis with five concentrations of 5FU and a solvent only control. 5FU was replenished with each media change.

Statistical Analysis

All experiments were performed from 3 independent passages, each consisting of either three or five biological replicates (different wells). Video bioinformatics assessment was performed from a total of 30 areas within three independent culture wells per replicate. For single and multiple comparisons, an unpaired student's T-test and a One-Way ANOVA with Holm-Sidak post-hoc analysis was performed, respectively. A *P*-value of 0.05 or smaller was considered statistically significant (SigmaPlot, Systat Software, San Jose, CA).

RESULTS

Pluripotency assessment of cell lines used

To apply hiPSC technology in the cell-based replacement of diseased or injured bone tissue or the screening for skeletal toxicity and teratogenicity, the osteogenic differentiation potential of human induced pluripotent stem cells must first be determined. To rule out that eventual differences in osteogenic differentiation capacity stemmed from differences in their pluripotency status, H9 hESCs and RIV4 and RIV9 hiPSCs were first compared for expression of pluripotency associated markers and absence of those associated with germ layer differentiation.

All lines displayed similar morphology and both hiPSC lines showed a normal karyotype (Fig. 1A, B). In the undifferentiated state, RIV9 and RIV4 lines expressed POU5F1, SOX2, and NANOG transcription factors, which localized to the nucleus, and the membrane-associated stage-specific embryonic antigen 4 (SSEA4; Fig. 1C). A quantitative comparison of pluripotency marker mRNA levels showed no statistical difference between the RIV and the H9 lines (Fig. 1D). Upon withdrawal of pluripotency conditions, all lines up-regulated the expression of tri-lineage genes (Fig. 1E–G), which were found at very low levels in the undifferentiated cells, concomitant with a reduction in pluripotency mRNAs with increased time in differentiation conditions (DMEM+FBS). These data indicated that all lines used in this study showed general tri-lineage potential facilitating the assessment of their osteogenic differentiation potential.

Characterization of osteoblast cells derived from hESCs

For osteogenic induction, we adopted a monolayer overgrowth culture approach previously described by Karp *et al.* [10] (for schematic see Fig. 2A) after attempts to execute an embryoid body-based protocol failed due to excessive cell death after replating (Supplemental Fig. 1A). We selected VD3 as an osteogenic supplement as it led to high levels of alkaline phosphatase (ALP) enzyme activity and superior calcification over DEX induction in pilot experiments (Supplemental Fig. 1B).

Upon VD_3 induction, differentiating ESCs showed black appearing deposits, which represent the calcification of the extracellular matrix, a hallmark of bone development from stem cells [46] (Fig. 2B). Cultures were positive for the major non-collagenous bone protein OCN and positive deposition of calcium ions was depicted by Alizarin Red S and Von Kossa stains (Fig. 2B). Quantitatively, the levels of deposited calcium rose over non-induced cultures by 10 days of the *in vitro* differentiation and had reached levels that were 78-fold higher than the non-osteogenic cells by day 30 (Fig. 2C). At late stages of osteogenesis, osteoblast-specific expression of *SATB2, RUNX2* and *OCN* transitioned into osteocyte-specific expression of *CAPG* and *DESTRIN* [48] (Fig. 2D).

During early differentiation, the co-expression of SOX10/PAX7 and SOX10/TWIST suggested the presence of neural crest cells [39] (Fig. 3A), while these were absent in uninduced control cultures. Further, $p75^{NTR}$-positive cells, often associated with migrating cranial neural crest cells [39, 49], were more abundant than in spontaneously differentiating cultures, and a few days later cells became positive for PDGFRα, which associates with mesenchymal cells, a subsequent step in maturation (Fig. 3B). In line with this observation the expression of *PAX7* and *TFAP2α*, two neural plate border specifier genes [48–51], were over 470- and 3160-fold up-regulated over undifferentiated cells (Fig. 3C). Mimicking the timely expression during neural crest development, *SOX10* and *ZIC3* were expressed slightly later. Subsequently, *DLX6*, which marks osteoprogenitors from the neural crest was significantly up-regulated over undifferentiated cells (Fig. 3C). In contrast, *T/Brachyury* (*T/BRA*, a pan-mesodermal gene) [52], peaked simultaneously with *PAX7* on day 5 of differentiation (Fig. 3D), but remained ~140-fold lower than that of *PAX7. PAX7* expression was also 98- and 49-fold greater than the levels of the neuroepithelial *SOX1* and *PAX6*, respectively (Fig. 2E), suggesting that hESCs primarily differentiated through a neural crest route.

Osteogenic Analysis of hiPSCs

We next tested whether the RIV9 and RIV4 cells also responded to VD_3 with osteogenic differentiation. On day 30 of the culture process, both the RIV9 and RIV4 osteogenic cultures indeed displayed the characteristic black deposits in brightfield microscopy indicative of the mineralized extracellular matrix produced by osteoblasts (Fig. 4A). This was further supported by positive immunostaining for OCN, Alizarin Red S, and von Kossa stains. Both RIV lines also showed measurable levels of inorganic phosphate and calcium (Fig. 4B, C). While these data suggested that all tested lines were generally capable of differentiating into osteoblasts, we noted an inconsistency in the mineralization process between H9, RIV9 and RIV4 during our studies. For example, inorganic phosphate was significantly decreased in the RIV4 cell line compared to the H9 cells (Fig. 4C, $P<0.05$), while both RIV4 and RIV9 lines showed less calcium content on day 20 ($P<0.05$) by multiple decades (Fig. 3B). Consequently, the Ca/P ratio, an important parameter in the determination of bone quality [53], was lower in both tested hiPSC lines, not even reaching values of 0.58 associated with fetal bone [53] (Fig. 3D). Only the Ca/P ratio for the H9 cells was determined at a close to physiological 2.6:1 [53–56].

We next examined when this difference first manifested itself. Morphological assessment suggested that both RIV4 and RIV9 cells calcified less than the H9 cells (Fig. 4D), and it appeared as if black deposit was visible earlier than in the H9 cells. Quantitative calcium measurements revealed significantly more calcification in RIV9 hiPSCs than in H9 hESCs on day 5, a pattern that reverted by day 15 (Fig. 4E). Instead, the inorganic phosphate content did not show any discernable pattern over a 20-day period (Fig. 4E).

To quantitatively determine this apparent difference in kinetics, we applied an innovative time-lapse morphometric assessment taking advantage of the black appearance of the calcium deposits in images [47]. Images of differentiating cultures were acquired every 12 hours over the course of 20 days and image segmentation applied to separate black pixels from the background. The remaining black pixels were used as a measure for calcification. Both RIV lines exhibited fewer dark pixels confirming a lower degree of calcification in the hiPSC lines (Fig. 4F). Calculating the calcification rate by charting the addition of black pixels as a function of elapsed time revealed that RIV4 and RIV9 appeared to calcify earlier than H9 cells (Fig. 4G). Together these data imply that hiPSC differentiations varied in the rate that calcification occurred at, with considerably lower osteogenic potential in the RIV4 and RIV9 lines.

Passage-to-passage analysis of osteogenic hPSC cultures

We next aimed to elucidate whether the noted variability in differentiation yield was due to differences in differentiation potential between passages or truly inherent in the specific line tested. To examine this variability more closely, we next compared three experiments inoculated from subsequent passages of cells (denoted by Roman numerals I–III) for osteogenic yield and levels of expression of genes associated with different levels of culture/osteoblast maturation.

The overall yield in calcium deposit followed a similar pattern of continuous up-regulation in all three cell lines, but was significantly lower in both RIV lines (H9>RIV9>RIV4, Fig. 5A). At the gene expression level, consistent patterns of expression that correlated between the three cell lines and with the calcification data were found for *OCN*, *PAX7* and *TWIST1* with the latter inversely correlating to calcification (Fig. 5B–D).

In contrast, no other examined genes exhibited any clear time- or cell-line dependent pattern of gene expression, although *RUNX2* and *OPN* indicated continuous maturation over time in the H9 cultures despite one out of the three passages under-expressing when compared to the other two (Supplemental Fig. A, B). Similarly, no time-dependent pattern could be observed for ALP enzyme activity or inorganic phosphate content (Supplemental Fig. 2E, F).

To test whether the observed differences between the three cell lines were correlative to passage variability, we next calculated the n-fold differences in gene expression, mineral content and enzyme activity across all time points and graphed them as box plots (Supplemental Fig. 3). These indicated that although some of the endpoints showed higher variability in the RIV9 cells, most of the endpoints exhibited equal variations in all cell lines, and none correlated with overall osteogenic yield.

Calcification ability of hPSCs correlates with PAX7 and TWIST1 expression and methylation status

Based on the association of *PAX7* and *TWIST1* expression measured in H9 ESCs (Fig. 2G) with neural crest lineage determination, and the correlative calcification kinetics found for H9 ESCs, we next comparatively measured the difference in mRNA expression patterns of multiple genes associated with the neural crest as well as mesodermal lineage across the three cell lines. *PAX7, TFAP2a, ZIC3* and *MSX2* mRNA levels were significantly lower in both RIV lines than in H9 cells (Fig. 6A). In contrast, the mesodermal genes *T/BRA*, *TBX6*, *MIXL1* and *MIER1* were expressed in the RIV9 line at 2-, 37-, 2- and 18-fold the levels found in H9 cells, respectively (Fig. 6A). Contrastingly, RIV4 cultures had lower levels than RIV9 of most of the neural crest and mesodermal genes, but highly expressed *SOX1* by 14-fold over the H9 line (Supplemental Fig. 4) potentially suggesting that their differentiation was halted at a neuroepithelial state [57]. H9 cultures with a CRISPR/Cas9-mediated disruption of T/BRA did not exhibit a reduction in calcification, while disruption of the same gene in RIV9 cells lessened the degree of calcification (Fig. 6B). This result potentially suggested that osteogenesis occurred independently of T/BRA in H9 cells, but was dependent on a mesodermal transition state in RIV9 cells.

Given that iPSCs have been reported to bear epigenetic marks from their cell type of origin [19] and given the high correlation between *PAX7* and *TWIST1* expression with the calcification yield in the H9 line over the RIV9 line we next examined the methylation status of both promoters. Methylation specific PCR supported the notion that the *PAX7* promoter region was hypomethylated in the H9 cells, while it was methylated in the RIV9 hiPSCs (Fig. 6C). This methylation pattern suggested that the activation of this locus was hindered in the RIV9 cells, which was reflected in the *PAX7* mRNA levels. In turn, the evaluation of the *TWIST1* promoter methylation status, a gene expressed by neural crest cells once they have committed to a mesenchymal fate, revealed high methylation of the *TWIST1* promoter in the H9 line, whereas *TWIST1* was less methylated in the RIV9 cell line (Fig. 6C). *In vivo*, *TWIST1* mediates cranial bone progenitor specification [58], and is highly expressed in mesenchymal cells and then down-regulated for further differentiation to occur [59, 60]. The detected methylation status on the *TWIST1* promoter suggested that in the RIV9 cells *TWIST1* was turned on prematurely, thwarting its proper activation pattern during differentiation. Indeed, already in undifferentiated RIV9 cells *TWIST1* was expressed 2.2–fold higher over the H9 hESCs (Fig. 6D) and increased with faster kinetics.

Next, we additionally analyzed the *PAX7* and *TWIST1* methylation status over a selection of different hESC and hiPSC lines and found differential methylation states that did not correlate with hESC or hiPSC identity (Supplemental Fig. 5). However, the methylation status of these two promoters in the undifferentiated state did seem to be predictive of the osteogenic differentiation capacity of the respective lines. Moreover, the methylation status also predicted the ability of two karyotypically abnormal RIV lines, RIV1 and RIV7, independently of their karyotypic abnormalities (Supplemental Fig. 5B–E). Together, these findings suggested that both *PAX7* and *TWIST1* methylation status may have a determining role in osteoblast development in PSCs.

RIV9 hiPSCs are able to predict skeletal teratogenesis despite their low osteogenic yield

While a low osteogenic differentiation potential of a pluripotent stem cell line could be of concern for its clinical application in cell-based regenerative medicine, it may still prove useful for the *in vitro* screening of putative skeletal toxicants despite its diminished osteogenic yield. To test this, we next examined the potential of the RIV9 line to accurately predict the toxicity of the strongly embryotoxic agent 5-Fluorouracil (5FU) [62] by assessing its inhibition of differentiation compared to its cytotoxicity [45]. The half-maximal inhibitory concentrations (ID_{50}) in the endpoint calcium content were not statistically different between the RIV9 and the H9 cells (P=0.090), neither were the half-maximal inhibitory concentrations of cytotoxicity (IC_{50}) (P=0.172) (Fig. 7A). Plotting the measured reduction in calcium content for every tested concentration in 5FU-treated osteogenic RIV9 cultures against the respective result found with the H9 cells (Fig. 7B) resulted in correlation coefficients close to 1, further demonstrating that RIV9 cells exhibit the same sensitivity to 5FU as H9 cells. These results potentially proved the usefulness of PSC osteogenic cultures in the prediction of skeletal toxicants, despite different differentiation kinetics or lower efficiencies.

DISCUSSION

In line with previous studies, we show here that hPSC cell lines are generally capable of osteogenic differentiation. However, to our knowledge this is the first report that VD_3, an osteogenic supplement that acts to trigger osteogenic gene expression and calcification in mouse and marmoset ESCs [6, 12], can also enhance human ESC osteogenic differentiation as well as induce osteogenic differentiation of human iPSCs. Notably, calcification levels were significantly lower in the two tested hiPSC lines than in the H9 hESC line. Where other studies have shown that osteoblasts can be derived from iPSCs when grown on scaffolds or with culture additives in general, most of these relied on qualitative von Kossa and Alizarin Red stains [8, 11]. Because only minimal quantitative analyses such as ALP and OCN were used in past studies [10], a thorough evaluation of the differences between hESCs and hiPSCs had not been performed [24, 63]. Using a broad range of techniques, including quantitative PCR, immunocytochemistry, and innovative video bioinformatics we show here systematically that although osteogenically differentiating hiPSCs can form a mineralized matrix, the two hiPSC lines tested exhibited lower osteogenic efficiency than H9 hESCs by multiple decades. While we initially hypothesized that this difference had to do with the type of cell studied we soon found evidence that these differences in osteogenic yield were cell type independent.

In contrast to the results presented here, a recently published study on mouse ESCs and two mouse iPSC lines did not identify any differences in osteogenic yield based on global gene expression analysis [73]. However, some data in another previous study hints at a lower osteogenic yield in both mouse and human iPSC lines [64]. Potentially, these discrepancies could be either based on species-specific differences of how differentiation proceeds or, alternatively, on the fact that some of the tested lines were grown on feeder cells while others were not, which may affect their pluripotency states. Indeed, future studies should examine whether returning all cell lines to naïve pluripotency would equalize the

methylation states of the key promoters analyzed here and thus level the osteogenic yield in all lines and potentially across species.

For now, the notably low differentiation yield in some hPSC lines may prove problematic in future applications for regenerative purposes. This is because large numbers of transplantable cells will be needed for any type of tissue repair [65, 66]. Hence, a low differentiation yield would render the already problematic scale-up even more labor-intensive. Of highest concern, however, is the fact there have so far been no investigations into the tissue origin of the osteoblasts that hPSCs generate. This is especially puzzling since it is well known that neural crest-derived frontal osteoblasts display a superior capacity to undergo osseous healing compared with calvarial osteoblasts of paraxial mesoderm origin [67]. In a grafting study, Leucht and colleagues showed that neural crest-derived bone would graft and give rise to new bone regardless of whether they were placed into a mandibular or tibial defect [33]. In contrast, tibial bone placed in the mandibular defect, the mesodermal tibial cells made cartilage in the mandible instead of bone. Jheon and Schneider [34] have further suggested that bone of neural crest origin will graft better when placed with its bone tissue of origin.

We suggest here for the first time that in some hPSCs osteoblasts may arise through a different embryonic lineage than in others. Specifically, differential regulation of *TWIST1* and *PAX7* mRNA expression caused by differential promoter methylation may be the apparent cause for defective neural crest osteogenesis in the RIV9 and RIV4 cell lines, which is otherwise found in H9 cells.

The low levels of *T/BRA* and *PAX7* expression in RIV4 hiPSCs potentially explains the decrease in RIV4 osteogenic yield, while positivity for *SOX1* could indicate that most of the RIV4 cells specify to neuroepithelium [57], but then fail to differentiate further. In contrast, *PAX7* and *SOX10* expression and stage-appropriate down-regulation of *TWIST1* mRNA correlate with a neural crest origin of H9-derived osteoblasts. Interestingly, the RIV9 cells highly expressed *T/BRA, TBX6*, *MIXL* and *MIER1* mRNA with decreased *PAX7*, *ZIC1* and *SOX1*, indicating a preference for mesodermal osteogenesis in those cells. We suggest this because mesendodermal differentiation is typically associated with a ~90-fold increase in the expression of *T/BRA* over undifferentiated cells [68], while in our cultures it is up-regulated only 3.5-fold. Emerging evidence suggests that presence *PAX7* may function to push cells towards a neural crest lineage [49, 50]. Our findings of *PAX7* gene expression and methylation status between the different human pluripotent stem cell lines coupled with high expression of *TFAP2a, ZIC1 and ZIC3* appears to support this notion. We show that H9 cells express higher levels of the *PAX7* gene coupled with an unmethylated promoter region. Thus, the RIV9 line could exhibit silencing of this locus through DNA methylation regulation.

We also concentrated on *TWIST1* as a candidate for assessing osteogenic potential because *TWIST1* seems to regulate the commitment of mesenchymally fated cells to the osteogenic lineage. While high *TWIST1* levels maintain mesenchymal stem cells in their unspecified state [60], silencing of *TWIST1* enhanced matrix mineralization and osteoblast gene expression in C3H10T1/2 cells [59]. In cranial cells, loss of *TWIST1* leads to the

maintenance of an epithelial character and reversal of EMT [69, 70]. Here we have revealed a potential role of gene-specific hypomethylation in limiting osteogenic differentiation of the RIV9 line, which may have caused the early overexpression of *TWIST1*.

One further indication for a possible alternative osteoblast origin between the H9 and the RIV9 cells was the kinetic calcification analysis that we performed. The video bioinformatic calcification data indicated that calcification arose quicker in the RIV9 line than in the H9 cells, validating findings by Nishikawa and colleagues, who had suggested a timely discrepancy between the appearance of neural crest and mesoderm-derived mesenchymal cells, whereby the mesoderm-derived mesenchymal progenitors appeared five days earlier than those derived from the neuroepithelium [57].

While the lower osteogenic output of some hPSC lines could mean that the development of an appropriate therapy for skeletal regeneration may require further investigations, this lower yield does not seem to preclude their use in the identification and prediction of the embryotoxicity associated with exposure to a chemical compound. Researchers are utilizing hPSCs increasingly for developmental toxicity testing, however there is a lack of different tissue endpoints such as bone [71]. Furthermore, the capacity of hiPSCs as a screening tool has not been explored [72]. We show here that hiPSCs may be potentially useful in the *in vitro* prediction of embryotoxicity even though a specific line may have a lower osteogenic yield.

CONCLUSION

In summary, our study demonstrates that different hPSC lines, including individual hiPSC clones, could have inherently different abilities to produce functional osteoblasts potentially based on the methylation marks placed on promotor regions important for lineage decisions. This could have an impact on the potential application domain of these cells. While low differentiation yields may be ameliorated by simple changes to the culturing protocol, for example EB-mediated differentiations or alternative supplements, future studies need to take into account the different capability of individual hPSC lines and characterize the process by which they lay down osteoblasts. Also, it will be important to investigate whether mesodermal-derived osteoprogenitors and hPSC-derived neural crest cells repair calvarial and long bone defects equally well.

Supplementary Material

Refer to Web version on PubMed Central for supplementary material.

Acknowledgments

The human ESC experiments were supported by a New Investigator Award to NzN (19KT-0017H) and a pre-doctoral fellowship to IKCM (20DT-0038) from the Tobacco Related Disease Research Program (TRDRP). Comparative studies with RIV9 hiPSCs were undertaken with support from the Center for Alternatives to Animal Testing (Johns Hopkins University, 2013-014) and RO1 DE025330 from the National Institutes of Health. NRLS is a TRDRP Cornelius Hopper Diversity and pre-doctoral fellowship Awardee (24DT-0002) and is supported by the International Foundation for Ethical Research. Human iPSCs were generated by the UCR Stem Cell Core Facility, which is a California Institute for Regenerative Medicine funded shared facility, and which provided that RIV karyotypes. The authors would like to thank Dr. Feodor Price (Harvard University), Dr. Derrick Rancourt (University of Calgary) and Dr. Amander Clark (University of California Los Angeles) for kindly sharing the hESC

and hiPSC lines (or genomic DNA thereof) analyzed in supplemental figure 2. The authors would like to thank Dr. Martín García-Castro for kindly donating SOX10 and PAX7 antibodies and Riley Bottom for technical assistance. The authors do not have any conflicts of interest to declare.

References

1. Dimos JT, Rodolfa KT, Niakan KK, et al. Induced pluripotent stem cells generated from patients with ALS can be differentiated into motor neurons. Science. 2008; 321:1218–1221. [PubMed: 18669821]
2. Mellough CB, Sernagor E, Moreno-Gimeno I, et al. Efficient stage-specific differentiation of human induced pluripotent stem cells toward retinal photoreceptor cells. Stem Cells. 2012; 30:673–686. [PubMed: 22267304]
3. Davis RP, Casini S, van den Berg CW, et al. Cardiomyocytes derived from pluripotent stem cells recapitulate electrophysiological characteristics of an overlap syndrome of cardiac sodium channel disease. Circulation. 2012; 125:3079–3091. [PubMed: 22647976]
4. McClelland-Descalzo DL, Ehnes DD, zur Nieden NI. Stem cells for osteodegenerative diseases: current studies and future outlook. Regen Med. 2014; 9:219–230. [PubMed: 24750062]
5. Buttery LD, Bourne S, Xynos JD, et al. Differentiation of osteoblasts and in vitro bone formation from murine embryonic stem cells. Tissue Eng. 2001; 7:89–99. [PubMed: 11224927]
6. zur Nieden NI, Kempka G, Ahr HJ. In vitro differentiation of embryonic stem cells into mineralized osteoblasts. Differentiation. 2003; 71:18–27. [PubMed: 12558600]
7. Ding H, Keller KC, Martinez IKC, et al. NO-β-catenin crosstalk modulates primitive streak formation prior to embryonic stem cell osteogenic differentiation. J Cell Sci. 2012; 125:5564–5577. [PubMed: 22946055]
8. Sottile V, Thomson A, McWhir J. In vitro osteogenic differentiation of human ES cells. Cloning Stem Cells. 2003; 5:149–155. [PubMed: 12930627]
9. Bielby RC, Boccaccini AR, Polak JM, et al. In vitro differentiation and in vivo mineralization of osteogenic cells derived from human embryonic stem cells. Tissue Eng. 2004; 10:1518–1525. [PubMed: 15588411]
10. Karp JM, Ferreira LS, Khademhosseini A, et al. Cultivation of human embryonic stem cells without the embryoid body step enhances osteogenesis in vitro. Stem Cells. 2006; 24:835–843. [PubMed: 16253980]
11. Bielby RC, Pryce RS, Hench LL, et al. Enhanced derivation of osteogenic cells from murine embryonic stem cells after treatment with ionic dissolution products of 58S bioactive solgel glass. Tissue Eng. 2005; 11:479–488. [PubMed: 15869426]
12. Trettner S, Findeisen A, Taube S, et al. Osteogenic induction from marmoset embryonic stem cells cultured in feeder-dependent and feeder-independent conditions. Osteoporosis Int. 2014; 25:1255–1266.
13. Yu J, Hu K, Smuga-Otto K, et al. Human induced pluripotent stem cells free of vector and transgene sequences. Science. 2009; 324:797–801. [PubMed: 19325077]
14. Kim D, Kim CH, Moon JI, et al. Generation of human induced pluripotent stem cells by direct delivery of reprogramming proteins. Cell Stem Cell. 2009; 4:472–476. [PubMed: 19481515]
15. Yu J, Vodyanik MA, Smuga-Otto K, et al. Induced pluripotent stem cell lines derived from human somatic cells. Science. 2007; 318:1917–1920. [PubMed: 18029452]
16. Takahashi K, Tanabe K, Ohnuki M, et al. Induction of pluripotent stem cells from adult human fibroblasts by defined factors. Cell. 2007; 131:861–872. [PubMed: 18035408]
17. Park IH, Zhao R, West JA, et al. Reprogramming of human somatic cells to pluripotency with defined factors. Nature. 2008; 451:141–146. [PubMed: 18157115]
18. Chin MH, Mason MJ, Xie W, et al. Induced pluripotent stem cells and embryonic stem cells are distinguished by gene expression signatures. Cell Stem Cell. 2009; 5:111–123. [PubMed: 19570518]
19. Kim K, Doi A, Wen B, et al. Epigenetic memory in induced pluripotent stem cells. Nature. 2010; 467:285–290. [PubMed: 20644535]

20. Ohi Y, Qin H, Hong C, et al. Incomplete DNA methylation underlies a transcriptional memory of somatic cells in human iPS cells. Nat Cell Biol. 2011; 13:541–549. [PubMed: 21499256]
21. Dolgin E. Gene flaw found in induced stem cells. Nature. 2010; 464:663. [PubMed: 20360708]
22. Nasu A, Ikeya M, Yamamoto T, et al. Genetically matched human iPS cells reveal that propensity for cartilage and bone differentiation differs with clones, not cell type of origin. PLoS One. 2013; 8:e53771. [PubMed: 23382851]
23. Sparks, NR., zur Nieden, NI. Pluripotent Stem Cells as Tools to Assess Developmental Toxicity: Diversity Instead of Consolidation. In: Sahu, SC., Casciano, DA., editors. Handbook of Nanotoxicology, Nanomedicine and Stem Cell Use in Toxicology. Chickester, UK: John Wiley & Sons; 2014. p. 299-307.
24. Guzzo RM, Gibson J, Xu RH, et al. Efficient differentiation of human iPSC-derived mesenchymal stem cells to chondroprogenitor cells. J Cell Biochem. 2013; 114:480–490. [PubMed: 22961870]
25. Deyle DR, Khan IF, Ren G, et al. Normal collagen and bone production by gene-targeted human osteogenesis imperfecta iPSCs. Mol Ther. 2011; 20:204–213. [PubMed: 22031238]
26. Quarto N, Leonard B, Li S, et al. Skeletogenic phenotype of human Marfan embryonic stem cells faithfully phenocopied by patient-specific induced-pluripotent stem cells. PNAS. 2011; 109:215–220. [PubMed: 22178754]
27. Lee TJ, Jang J, Kang S, et al. Mesenchymal stem cell-conditioned medium enhances osteogenic and chondrogenic differentiation of human embryonic stem cells and human induced pluripotent stem cells by mesodermal lineage induction. Tissue Eng Part A. 2014; 20:1306–1313. [PubMed: 24224833]
28. de Peppo GM, Marcos-Campos I, Kahler DJ, et al. Engineering bone tissue substitutes from human induced pluripotent stem cells. PNAS. 2013; 110:8680–8685. [PubMed: 23653480]
29. Tang M, Chen W, Liu J, et al. Human induced pluripotent stem cell-derived mesenchymal stem cell seeding on calcium phosphate scaffold for bone regeneration. Tissue Eng Part A. 2014; 20:1295–1305. [PubMed: 24279868]
30. Zou L, Luo Y, Chen M, et al. A simple method for deriving functional MSCs and applied for osteogenesis in 3D scaffolds. Sci Rep. 2013; 3:2243. [PubMed: 23873182]
31. Ardeshirylajimi A, Hosseinkhani S, Parivar K, et al. Nanofiber-based polyethersulfone scaffold and efficient differentiation of human induced pluripotent stem cells into osteoblastic lineage. Mol Biol Rep. 2013; 40:4287–4294. [PubMed: 23657591]
32. Kim MJ, Son MJ, Son MY, et al. Generation of human induced pluripotent stem cells from osteoarthritis patient-derived synovial cells. Arthritis Rheum. 2011; 63:3010–3021. [PubMed: 21953087]
33. Leucht P, Kim JB, Amasha R, et al. Embryonic origin and Hox status determine progenitor cell fate during adult bone regeneration. Development. 2008; 135(17):2845–54. [PubMed: 18653558]
34. Jheon AH, Schneider RA. The cells that fill the bill: neural crest and the evolution of craniofacial development. J Dent Res. 2009; 88(1):12–21. [PubMed: 19131312]
35. Park S, Im GI. Embryonic stem cells and induced pluripotent stem cells for skeletal regeneration. Tissue Eng Part B Rev. 2014; 20:381–391. [PubMed: 24206162]
36. Chatterjee P, Cheung Y, Liew CG. Transfecting and nucleofecting human induced pluripotent stem cells. J Vis Exp. 2011; 56:e3110.
37. Torrez LB, Perez Y, Yang J, et al. Derivation of neural progenitors and retinal pigment epithelium from common marmoset and human pluripotent stem cells. Stem Cells Int. 2012; 201:417865.
38. Kuske B, Savkovic V, zur Nieden NI. Improved media compositions for the differentiation of embryonic stem cells into osteoblasts and chondrocytes. Methods Mol Biol. 2011; 690:195–215. [PubMed: 21042995]
39. Betters E, Liu Y, Kjaeldgaard A, et al. Analysis of early human neural crest development. Dev Bio. 2010; 344:578–592. [PubMed: 20478300]
40. Davis LA, Dienelt A, zur Nieden NI. Absorption-based assays for the analysis of osteogenic and chondrogenic yield. Methods Mol Biol. 2011; 690:255–272. [PubMed: 21042998]
41. Majumdar S, Ramachandran S, Cerione RA. New insights into the GTP binding/GTP hydrolytic cycle of large G proteins. J Biol Chem. 2006; 281:9219–9226. [PubMed: 16469737]

42. Livak KJ, Schmittgen TD. Analysis of relative gene expression data using real-time quantitative PCR and the 2(−Delta C(T)). Method Methods. 2001; 25:402–408. [PubMed: 11846609]
43. Leung AW, Murdoch B, Salem AF, et al. WNT/β-catenin signaling mediates human neural crest induction via a pre-neural border intermediate. Development. 2016; 143(3):398–410. [PubMed: 26839343]
44. Sung CO, Lee KW, Han S, et al. Twist1 is up-regulated in gastric cancer-associated fibroblasts with poor clinical outcomes. Am J Pathol. 2011; 179:1827–1838. [PubMed: 21854747]
45. Kuske, B., Pulyanina, PY., zur Nieden, NI. Embryonic Stem Cell Test: Stem Cell Use in Predicting Developmental Cardiotoxicity and Osteotoxicity. In: Harris, C., Hansen, JM., editors. Developmental Toxicology: Methods in Molecular Biology. Vol. 889. 2012. p. 147-179.
46. zur Nieden NI, Price FD, Davis LA, et al. Gene profiling on mixed embryonic stem cell populations reveals a biphasic role for beta-catenin in osteogenic differentiation. Mol Endocrinol. 2007; 21:674–685. [PubMed: 17170073]
47. zur Nieden NI, Davis LA, Rancout DE. Monolayer cultivation of osteoprogenitors shortens duration of the embryonic stem cell test while reliably predicting developmental osteotoxicity. Toxicology. 2010; 277:66–73. [PubMed: 20817070]
48. Guo D, Keightley A, Guthrie J, et al. Identification of osteocyte-selective proteins. Proteomics. 2010; 10:3688–3698. [PubMed: 20845334]
49. Basch ML, Bronner-Fraser M, García-Castro MI. Specification of the neural crest occurs during gastrulation and requires Pax7. Nature. 2006; 441:218–222. [PubMed: 16688176]
50. Murdoch B, DelConte C, García-Castro MI. Pax7 lineage contributions to the mammalian neural crest. PLoS One. 2012; 7:e41089. [PubMed: 22848431]
51. Li W, Cornell RA. Redundant activities of Tfap2a and Tfap2c are required for neural crest induction and development of other non-neural ectoderm derivatives in zebrafish embryos. Dev Biol. 2007; 304(1):338–354. [PubMed: 17258188]
52. Beddington RS, Rashblass P, Wilson V. Brachyury--a gene affecting mouse gastrulation and early organogenesis. Dev Suppl. 1992:157–165. [PubMed: 1299362]
53. Sornay-Rendu E, Munoz F, Garnero P, et al. Identification of osteopenic women at high risk of fracture: the OFELY study. J Bone Miner Res. 2005; 20:1813–1819. [PubMed: 16160738]
54. Sotiropoulou P, Fountos G, Martini N, et al. Bone calcium/phosphorus ratio determination using dual energy X-ray method. Phys Med. 2015; 31:307–313. [PubMed: 25726476]
55. Tzaphlidou M, Zaichick V. Calcium, phosphorus, calcium-phosphorus ratio in rib bone of healthy humans. Biol Trace Elem Res. 2003; 93:63–74. [PubMed: 12835491]
56. Quelch KJ, Melick RA, Bingham PJ, et al. Chemical composition of human bone. Arch Oral Biol. 1983; 28:665–674. [PubMed: 6314948]
57. Takashima Y, Era T, Nakao K, et al. Neuroepithelial cells supply an initial transient wave of MSC differentiation. Cell. 2007; 129:1377–1388. [PubMed: 17604725]
58. Yen HY, Ting MC, Maxson RE. Jagged1 functions downstream of Twist1 in the specification of the coronal suture and the formation of a boundary between osteogenic and non-osteogenic cells. Dev Biol. 2010; 347:258–270. [PubMed: 20727876]
59. Miraoui H, Severe N, Vaudin P, et al. Molecular silencing of Twist1 enhances osteogenic differentiation of murine mesenchymal stem cells: implication of FGFR2 signaling. J Cell Biochem. 2010; 110:1147–1154. [PubMed: 20564211]
60. Goodnough LH, Chang AT, Treloar C, et al. Twist1 mediates repression of chondrogenesis by β-catenin to promote cranial bone progenitor specification. Development. 2012; 139:4428–4438. [PubMed: 23095887]
61. Draper JS, Smith K, Gokhale P, Moore HD, Maltby E, Johnson J, Meisner L, Zwaka TP, Thomson JA, Andrews PW. Recurrent gain of chromosomes 17q and 12 in cultured human embryonic stem cells. Nat Biotechnol. 2004; 22(1):53–54. [PubMed: 14661028]
62. Romero A, Vilanova E, Sogorb MA. Shortening and improving the embryonic stem cell test through the use of gene biomarkers of differentiation. J Toxicol. 2011:286034. [PubMed: 21876691]

63. Liu Y, Goldberg AJ, Dennis JE, et al. One-step derivation of mesenchymal stem cell (MSC)-like cells from human pluripotent stem cells on a fibrillar collagen coating. PLoS One. 2012; 7:e33225. [PubMed: 22457746]

64. Kanke K, Masaki H, Saito T, et al. Stepwise Differentiation of Pluripotent Stem Cells into Osteoblasts Using Four Small Molecules under Serum-free and Feeder-free Conditions. Stem Cell Rep. 2014; 2:751–760.

65. Diekman BO, Christoforou N, Willard VP, et al. Cartilage tissue engineering using differentiated and purified induced pluripotent stem cells. PNAS. 2012; 109:19172–19177. [PubMed: 23115336]

66. Yoshida Y, Yamanaka S. Recent stem cell advances: induced pluripotent stem cells for disease modeling and stem cell-based regeneration. Circulation. 2010; 122:80–87. [PubMed: 20606130]

67. Quarto N, Wan DC, Kwan MD, et al. Origin matters: differences in embryonic tissue origin and Wnt signaling determine the osteogenic potential and healing capacity of frontal and parietal calvarial bones. J Bone Miner Res. 2010; 25:1680–1694. [PubMed: 19929441]

68. Singh AM, Reynolds D, Cliff T, et al. Signaling network crosstalk in human pluripotent cells: a Smad2/3-regulated switch that controls the balance between self-renewal and differentiation. Cell Stem Cell. 2012; 10:312–26. [PubMed: 22385658]

69. Bildsoe H, Loebel DA, Jones VJ, et al. Requirement for Twist1 in frontonasal and skull vault development in the mouse embryo. Dev Biol. 2009; 331:176–188. [PubMed: 19414008]

70. Bildsoe H, Loebel DA, Jones VJ, et al. The mesenchymal architecture of the cranial mesoderm of mouse embryos is disrupted by the loss of Twist1 function. Dev Biol. 2013; 374:295–307. [PubMed: 23261931]

71. Krug AK, Kolde R, Gaspar JA, et al. Human embryonic stem cell-derived test systems for developmental neurotoxicity: a transcriptomics approach. Arch Toxicol. 2013; 87:123–143. [PubMed: 23179753]

72. Scott CW, Peterts MF, Dragan YP. Human induced pluripotent stem cells and their use in drug discovery for toxicity testing. Toxicol Lett. 2013; 219:49–58. [PubMed: 23470867]

73. Ma MS, Kannan V, de Vries AE, et al. Characterization and comparison of osteoblasts derived from mouse embryonic stem cells and induced pluripotent stem cells. J Bone Miner Metab. 2017; 35(1):21–30. [PubMed: 26747612]

HIGHLIGHTS

- Active Vitamin D3 induces osteogenesis in multiple human ESC and iPSC lines
- In H9 hESCs vitamin D3 mainly derives osteoblasts from the neural crest
- Calcification yield is lower in RIV9 cells, while calcification kinetics are accelerated
- Calcification deficiency correlated with levels of *OCN*, *PAX7* and *TWIST1* mRNAs

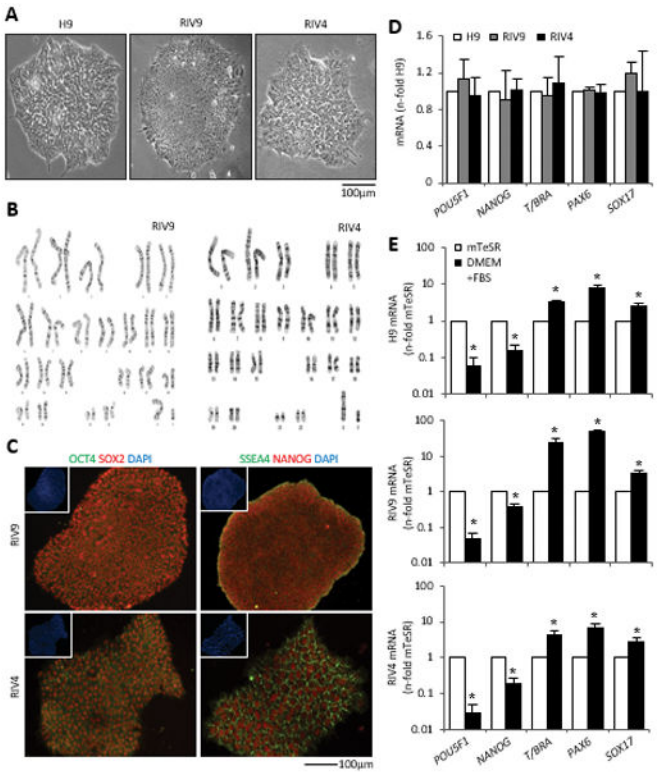

Figure 1. Cytogenetic, pluripotent, and genetic characterization of hiPSC lines

(A) Morphology of H9 hESCs and RIV9 and RIV4 hiPSCs.

(B) Cytogenetic G-banding analysis for RIV9 and RIV4 hiPSCs (46, XY).

(C) Immunofluorescence staining for pluripotent markers. *Insets*, Nuclear counterstaining with DAPI.

(D) qPCR for mRNA expression of pluripotency and lineage markers on undifferentiated hPSCs. Expression is normalized to H9 hESCs and standardized to *GAPDH,* n=3 independent samples ± SD.

(E–G) qPCR mRNA expression of the same set of mRNAs on differentiating hPSCs, normalized to *GAPDH*, n=3 independent samples ± SD. **P*<0.05, Student's t-test compared to expression in undifferentiated cells (mTeSR).

T/BRA, T-Brachyury; GAPDH, glyceraldehyde 3-phosphate dehydrogenase.

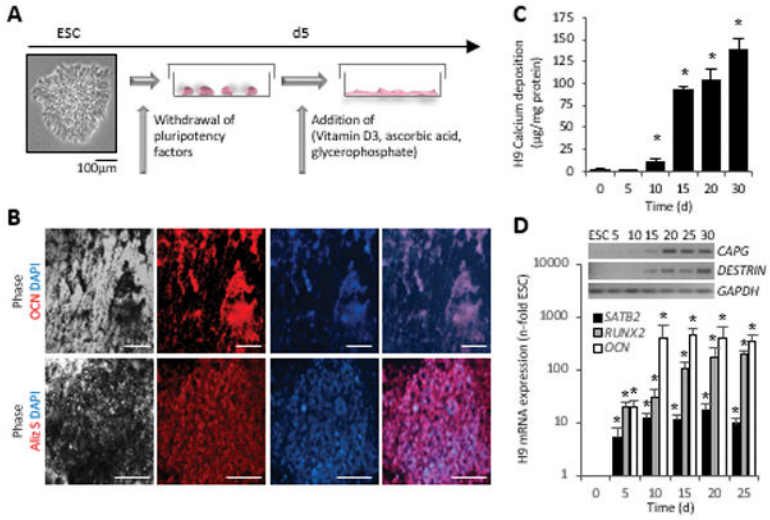

Figure 2. Osteogenic differentiation of hESCs

(A) Schematic of the osteogenic induction protocol.

(B) Immunostaining with an osteocalcin antibody reveals presence of bone matrix in the vicinity of black deposits. Alizarin Red S staining detected calcium ions in the same areas. Scale bars = 100 µm.

(C) Quantitative measurement of deposited calcium over time, n=5 independent replicates ± SD, **P*<0.05 Student's t test compared to d0.

(D) Quantitative mRNA analysis of *RUNX2, SATB2* and *OCN*, normalized to *GAPDH* (n=3 independent samples ± SD), **P*<0.05 One-Way ANOVA over day 0. Triplicates were pooled for RT-PCR analyses of the osteocyte genes *CAPG* and *DESTRIN* (inset).

OCN, osteocalcin; Aliz S, Alizarin Red S; GAPDH, glyceraldehyde 3-phosphate dehydrogenase.

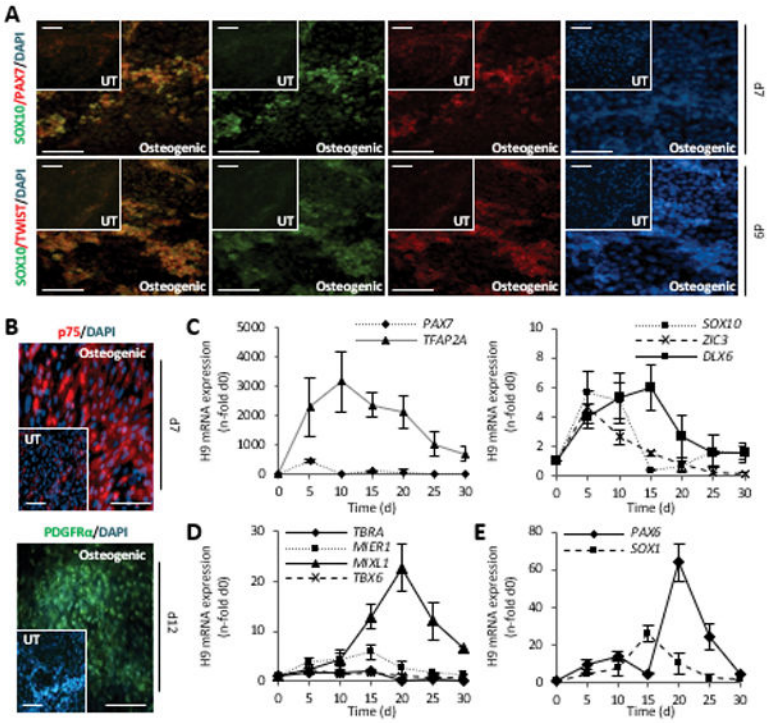

Figure 3. Intermediate differentiation in H9 cells is through the neural crest lineage

(A, B) Double staining with antibodies against SOX10/PAX7, SOX10/TWIST1, and single stains with $p75^{NTR}$, and PDGFRα at indicated time points of differentiation. Scale bar = 100 μm.

(C–E) Quantitative mRNA analysis of early lineage genes, normalized to *GAPDH,* n=3 independent samples ± SD.

T/BRA, T-Brachyury; GAPDH, glyceraldehyde 3-phosphate dehydrogenase.

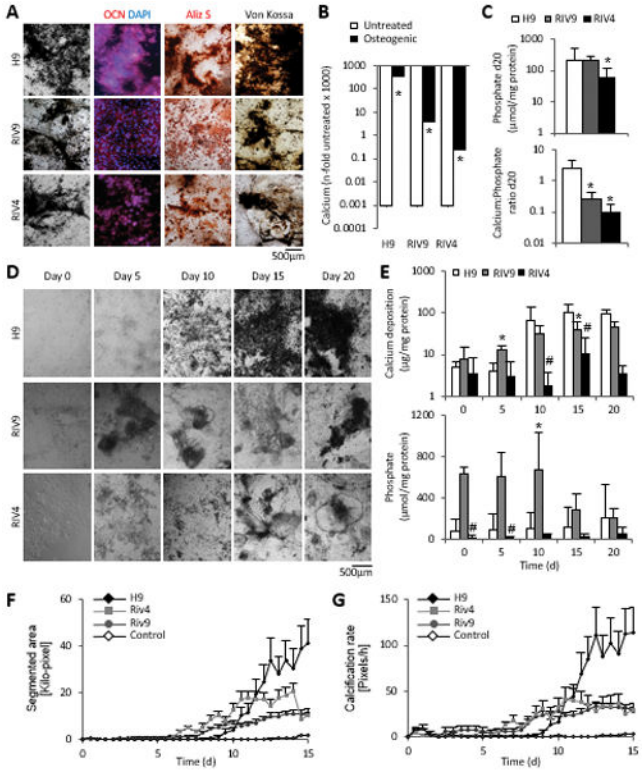

Figure 4. Osteogenic differentiation in RIV9 and RIV4 hiPSCs

(A) Photomicrographs of unstained and stained osteogenic cultures from H9 hESCs and RIv9 and RIV4 hiPSCs on day 30 of differentiation. Matrix mineralization detected with OCN, Aliz S, and Von Kossa stains.

(B) 20-day-old osteogenic hPSCs deposit significant levels of calcium ions over spontaneously differentiating cultures (n=5 independent samples ± SD). **P*<0.05 One-Way ANOVA over spontaneous differentiations.

(C) Levels of inorganic phosphate levels measured with the PiPer assay on day 20 content, n=5 independent samples ± SD, **P*<0.05 One-Way ANOVA over H9. Bottom graph depicts calcium:phosphate ratios determined from Ca^{2+} and PiPer assays, day 20, n=3 independent replicates ± SD. **P*<0.05 One-Way ANOVA versus H9.

(D) Morphological time course of hPSC osteogenic differentiation reveals differences in calcification yield between different hPSC lines.

(E) Calcification time course analysis shows heterogeneity between osteogenesis in different hPSC lines. Levels of inorganic phosphate also vary depending on differentiation day; n=3 independent replicates ± SD. #*P*<0.05 RIV9-H9; **P*<0.05 RIV4-H9, One-way ANOVA.

(F, G) RIV9 and RIV4 cultures begin their calcification process earlier than H9 cells as determined by video bioinformatics analysis, n=10 technical replicates from three biological replicates±SEM.

OCN, osteocalcin; Aliz S, Alizarin Red S.

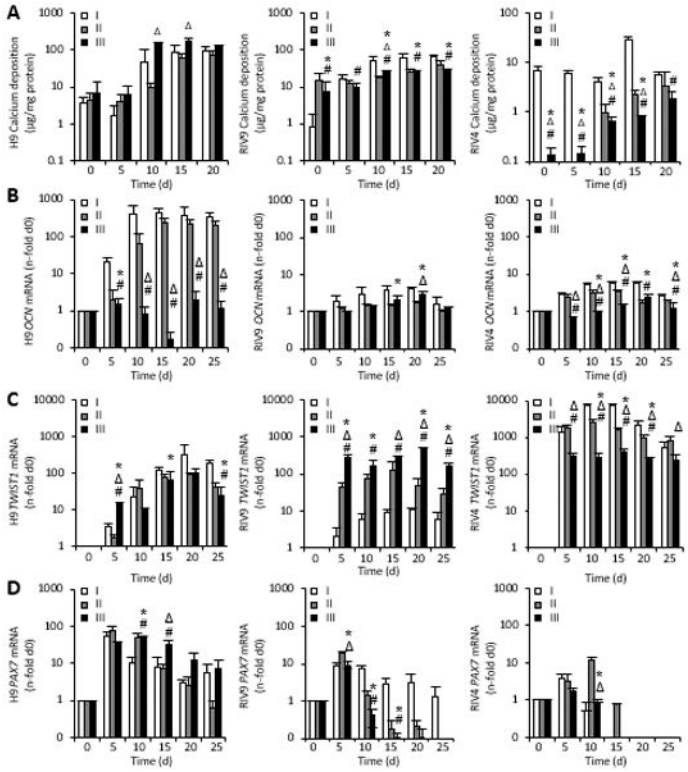

Figure 5. Passage-specific analysis of bone parameters and gene expression

(A). Calcium content in hPSC cultures inoculated from three different passages (I–III). Data points represent 5 technical replicates for each biological passage shown ± SD. **P*<0.05 passage II over I; #*P*<0.05 passage III over I; Δ*P*<0.05 passage III over II.

(B–D) The mRNA expression of osteogenic genes was determined with qPCR and normalized to *GAPDH*, n=3±SD. RIV9 and RIV4 hiPSCs failed to show definitive osteogenic patterns. **P*<0.05 passage II over I; #*P*<0.05 passage III over I; Δ*P*<0.05 passage III over II, One-way ANOVA.

OCN, osteocalcin; GAPDH, glyceraldehyde 3-phosphate dehydrogenase.

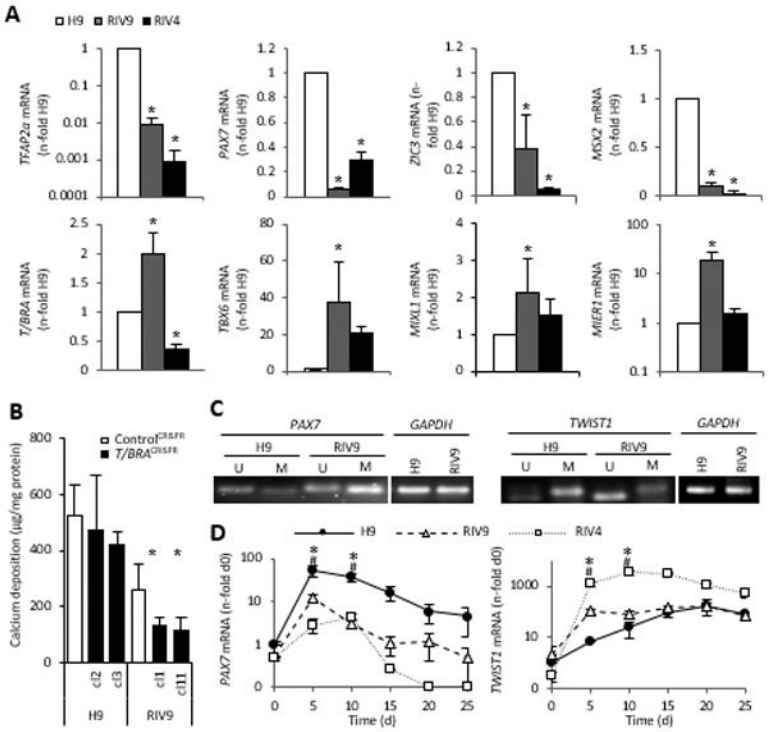

Figure 6. Osteoblast origin correlates with methylation of the *TWIST1* and *PAX7* promoters

(A) mRNA expression for genes associated with mesoderm or the neural crest was quantitatively analyzed with qPCR, n=3 independent samples ± SD. **P*<0.05 One-way ANOVA over H9.

(B) Quantification of calcium content in control cultures of H9 and RIV9 cells and two clones each with a CRISPR–Cas9-mediated disruption of T/BRACHYURY (*T/BRA*^{CRISPR}). Values represent means of three independent experiments, n=5 technical replicates each ± SD. **P*<0.05 One-way ANOVA versus the respective control ^{CRISPR} cell line.

(C) Methylation-specific PCR showed that *TWIST1* was unmethylated (U) in the RIV9 line. The *PAX7* promoter region was methylated (M) in the RIV9 line.

(D) Quantitative analyses of time course mRNA expression in the RIV9 and H9 cells, normalized to *GAPDH*, pooled from n=3 independent replicates ± SD. #*P*<0.05 RIV9-H9; **P*<0.05 RIV4-H9, One-way ANOVA.

T/BRA, T-Brachyury; GSC, Goosecoid; GAPDH, glyceraldehyde 3-phosphate dehydrogenase; M, methylated; U, unmethylated.

A

5-Fluorouracil				
	H9 hESC		RIV9 hiPSC	
	IC_{50} µg/mL	± SD	IC_{50} µg/mL	± SD
I	0.0002	0.00005	0.00015	0.00005
II	0.00025	0.00005	0.000175	0.00002
III	0.00016	0.00003	0.000163	0.00002
	ID_{50} µg/mL	± SD	ID_{50} µg/mL	± SD
I	0.00025	0.00006	0.00043	0.000005
II	0.0004	0.00001	0.0004	0.00001
III	0.0003	0.00001	0.00045	0.000005

B

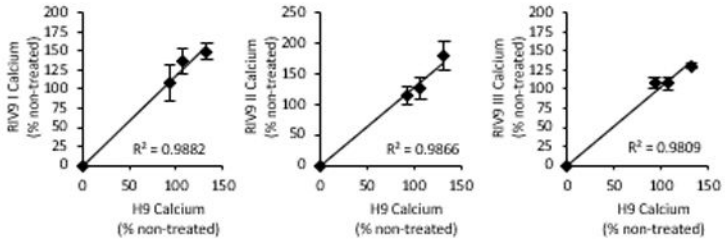

Figure 7. Toxicity of 5FU tested with H9 and RIV9 hPSCs

(A) Table of half-maximal inhibitory doses for cytotoxicity (IC_{50}) as determined from concentration-response curves with MTT assay and differentiation (ID_{50}) with calcium assay. (B) Linear regression of RIV9 half-maximal inhibition of differentiation graphed against H9 half-maximal inhibition of differentiation. Both cell lines showed similar classification in predicting skeletal toxicity of 5FU. 5FU, 5-fluorouracil; MTT, 3-[4,5-dimethylthiazol-2-yl]-2,5-diphenylterazolium bromide.